Carpathian Journal of Earth and Environmental Sciences, November 2013, Vol. 8, No. 4, p. 125 - 138

METAMORPHISM AND GEOCHEMICAL ASPECTS ON NEOPROTEROZOIC SERPENTINITES HOSTED CHROME SPINEL FROM GABAL AL-DEGHEIMI, EASTERN DESERT, EGYPT

Sherif KHARBISH

Geology Department, Faculty of Science, Suez University, Suez, 43518, Egypt; e-mail: sherifkhabrish@hotmail.com

Abstract: Petrographic and geochemical studies of the chrome (Cr)-spinel in serpentinites from the Gabal Al-Degheimi, in the central Eastern Desert of Egypt, are made to evaluate their textural and compositional variations Cr-spinel cores do not appear to have re-equilibrated completely with the metamorphic spinel rims and surrounding silicates, suggesting relic magmatic composition unaffected by metamorphism. Accessory Cr-spinel in the serpentinites is characterized by Cr (0.60-0.78) and Mg (0.54-0.68). Normalized REE patterns and the low abundances of Ti, Na, Nd, Sm, Lu and Hf of serpentinites and Cr-spinel core compositions suggest that Gabal Al-Degheimi serpentinites are of ophiolitic origin and represent relicts of a reduced depleted harzburgite to dunite mantle peridotites formed in an oceanic suprasubduction zone (marginal-basin) tectonic environment that experienced high degrees of partial melting in excess of 22%. Textural and compositional features of the Cr-spinels suggest transitional greenschist-amphibolite up to lower amphibolite facies metamorphism, which is isofacial with the country rocks.

Key Words: Cr-spinel, Gabal Al-Degheimi serpentinites, mineral chemistry, Ophiolites

1. INTRODUCTION

Serpentinites, which are particularly common in the central and southern sectors of the Eastern Desert (ED) of Egypt (870 to 690 Ma; Stern et al., 2004), constitute the major part of the Egyptian ophiolites (Shackleton et al., 1980). The Egyptian serpentinites derived from peridotites (Aly et al., 1995) and were classified into (1) allochthonous serpentinites, including mélanges and (2) flow intruded serpentinites (Akaad & Abu El Ela, 2002).

Because serpentinites contain traces of their history, they deserve detailed study, notwithstanding the difficult task of deriving information from these complex rocks. These traces may be extracted from the composition of unaltered chrome (Cr-) spinel or chromite more easily than from bulk data. Cr-spinel which is considered a common accessory mineral in mafic and ultramafic rocks, displays a large compositional range reflecting their primary origin. Magmatic Cr-spinel chemistry is sensitive to unaltered melt composition, crystallization pressure and the degree of melting in the mantle source region. Therefore, Cr-spinels, refractory and resistant to alteration, are reliable petrogenetic indicators (Barnes & Roeder, 2001) and capable of recording their magmatic history. However, primary Cr-spinels may re-equilibrate with surrounding silicates during metamorphic or hydrothermal processes (Kimball, 1990), thus possibly producing spinel compositions that have no bearing upon the magmatic history (Merlini et al., 2009).

Cr-spinel is a member of the spinel group whose ideal formula is defined as $R^{2+}OR^{3+}O_3$ where, $R^{2+} = Mg^{2+}$, Fe^{2+}, Mn^{2+} and Ni and $R^{3+} = Cr^{3+}$, Al^{3+} and Fe^{3+} (Deer et al., 1992). The unit cell of Cr-spinels is defined as sheets of oxygen anions roughly packed in a cubic shape containing 24 cations distributed between tetrahedral (A) and octahedral (B) sites. The distribution of cations between A and B sites in the unit cell determines the two structural types of spinel: (1) normal spinels where the eight tetrahedral sites are occupied by R^{2+} cations and the 16 octahedral sites are occupied by R^{3+} cations; and (2) inverse spinels where the eight tetrahedral sites are occupied by R^{3+} cations and the 16 octahedral sites are occupied by both R^{2+} and R^{3+} cations in a 1:1 ratio (Deer et al., 1992).

The present work examines the effects of serpentinization and metamorphism on the

composition of Cr-spinel and its alteration rims in serpentinites from the Gabal Al-Degheimi, central ED, Egypt. In addition, the composition of primary Cr-spinels and bulk-rock major and trace elements are used to assess the petrogenesis and tectonic setting of the Gabal Al-Degheimi serpentinites (GDS).

2. GEOLOGY AND PETROGRAPHY

The area of GDS (Fig. 1) is occupied by older ophiolite assemblage (serpentinites, talc carbonates, metagabbros and metavolcanics) incorporated within the younger metavolcanic-metasedimentary island-arc association, together with syn- to late-orogenic calc-alkaline granitoids, post-orogenic alkaline granites and Dokhan volcanics (Akaad & Abu El-Ela, 1996). GDS are generally medium-grained homogeneous massive rocks but became sheared and foliated near the contacts (Fig. 2a). The sheared serpentinites have the same mineralogical composition as the massive varieties, but the minerals in the former are commonly arranged in subparallel alignment producing the schistosity. Alteration of serpentinites into dark brown and buff colored talc–carbonate rocks is rather common (Fig. 2a) and these occur either as scattered patches or sheet-like bodies along shear zones and fault planes within the serpentinite masses.

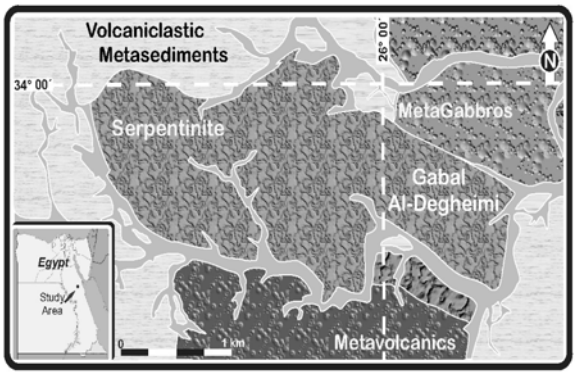

Figure 1. Geologic map of the Gabal Al-Degheimi, central ED of Egypt.

Petrographically, GDS consist essentially of fibrous flakes of serpentine minerals together with Cr-spinels, chlorite and minor amounts of carbonates. They commonly preserve psuedomorphs of orthopyroxene and olivine, indicating harzburgite and dunite composition of the parent rocks; harzburgite dominates over dunite. The original orthopyroxene and olivine are indicated by the presence of bastite and serpentine mesh textures (Fig. 2b), respectively. Chlorite occurs as small aggregates in a serpentine matrix or as aureoles around altered Cr-spinels as well as coating bastite and mesh textures, indicating that chlorite formed after serpentinization. Carbonates occur as sparse crystals and fine aggregates in the massive serpentinites or as veinlets and pockets in the sheared varieties.

Spinel grains occur as irregular to amoeboid shapes and display three irregular optical zoning: the core (dark gray color in thin section when viewed under SEM) represents unaltered primary Cr-spinel, the intermediate zone (gray) corresponds to Cr-spinel altered to “ferritchromite” and the outer rim (light gray) is Cr-magnetite (Fig. 2c, d).

3. SAMPLES AND EXPERIMENTS

Mineral compositions were obtained by electron microprobe using a Cameca SX 100 instrument at the Lithospheric Research Department, Vienna University (VU), Austria. Excitation voltage was 20 kV and beam current was 15 nA. Most elements were measured with a counting time of 10s. Calibrations were performed using natural and synthetic reference materials: chromite (Cr, Al, Fe), periclase (Mg), rhodonite (Mn) and rutile (Ti).

Bulk rock major and trace elements were measured by XRF at Lithospheric Research Department, VU, using a Philips PW 2400 spectrometer. Loss on ignition was determined after igniting 5g of sample powder in porcelain crucibles at 1050°C for 1h. Analytical precision is better than 1% and 3% for major and trace elements, respectively. The REE were analyzed using Elan 6100 ICP-MS with Mercury Flow Injection System "FIMS 100" and Laser Sampler "LSX 200" at the Environmental Geosciences Department, VU, Austria.

The Raman spectra of serpentine minerals were collected in the spectral range from 10 to 1200 cm^{-1} by using a Renishaw RM1000 confocal notch filter-based micro-Raman system at the Institute of Mineralogy and Crystallography, Vienna University, Austria. The 632.8 nm (HeNe Laser) excitation line of a 17 mW solid state laser with polarisation extinction > 500:1 was focused with a 50x /0.75 objective on the sample surface. The back-scattered radiation was analyzed with a 1200 lines/mm grating monochromator. Raman intensities were collected with a thermo-electrically cooled CCD array detector. The resolution of the system was 2 cm^{-1}, the wavenumber accuracy was ±1 cm^{-1} (both calibrated with the Rayleigh line and the 520.5 cm^{-1} line of a Si standard). Instrument control and data acquisition were done with GRAMS/32 software. Depending on the signal intensity, accumulations with 120 m per "spectral window” (i.e., exposure time of the detector) were measured.

4. RESULTS

4.1. Spinel chemistry

Representative EMA of Cr-spinel and their alteration rims from the GDS are given in Table 1. Chemical data sharply plot into three groups (i.e. magmatic Cr spinels, ferritchromite and Cr-magnetite (Fig. 3a) that mark the discontinuous change from magmatic Cr spinels to altered rims.

Magmatic Cr-spinel is chemically homogeneous, having very little compositional variation. Its composition is characterized by Fe^{2+}-rich Cr-spinel where $Cr/Fe^{2+}>1$ (Table 1). $Fe^{2+} = [Fe^{2+}/(Fe^{2+} + Mg)]$ ranges from 0.32 to 0.46, whereas $Cr = [Cr/(Cr+Al]$ varies between 0.60 and 0.78 (Table 1). The Cr_2O_3 ranges from 46.89 to 55.74 wt% and is inversely correlated with Al_2O_3, which ranges from 10.71 to 20.84 wt%. Some substitution between Fe^{2+} and Mg^{2+} is also seen. $Mg = [Mg/(Mg+Fe^{2+})]$ (Table 1), ranges from 0.54 to 0.68 and $Fe^{3+} = [Fe^{3+}/(Fe^{3+}+Cr+Al)]$ is lower than 0.07, corresponding to Fe_2O_3 contents between 3.33 and 6.14 wt%. TiO_2 (<0.29wt%) and MnO (< 0.77 wt%) concentrations are low. This composition is interpreted to be characteristic of primary Cr-spinel with no or very little post-compositional change.

The altered spinel rims of metamorphic origin, including ferritchromit and Cr-magnetite lie along the $Cr–Fe^{3+}$ join on the $Cr–Al–Fe^{3+}$ diagram (Fig. 3a). Ferritchromit have a chemical composition (Table 1) that provides evidence of an alteration event characterized by Fe_2O_3 enrichment and Cr# increase (caused by loss of Al_2O_3) with little or no variation in FeO and MgO contents (Fig. 3b). These compositions are typical for a Fe^{3+}-rich, Cr spinel known in the literature as "ferritchromite" (Evans & Frost, 1975). The Cr-magnetite ($Cr/Fe^{2+}<1$; Table 1) display a chemical composition, similar to that described in the ferritchromit in terms of Fe_2O_3, Cr and Al_2O_3, but showing FeO- enrichment and Mg decrease, due to the extensive $Mg\text{-}Fe^{2+}$ exchange (Fig. 3b).

This composition is identified as a Cr-magnetite rather than primary magnetite or Cr-spinel. According to Barnes & Roeder (2001) primary magnetite plots along the $Al–Fe^{3+}$ join of the $Cr–Al–Fe^{3+}$ whereas metamorphic magnetite lie along $Cr–Fe^{3+}$ join (Fig. 3a).

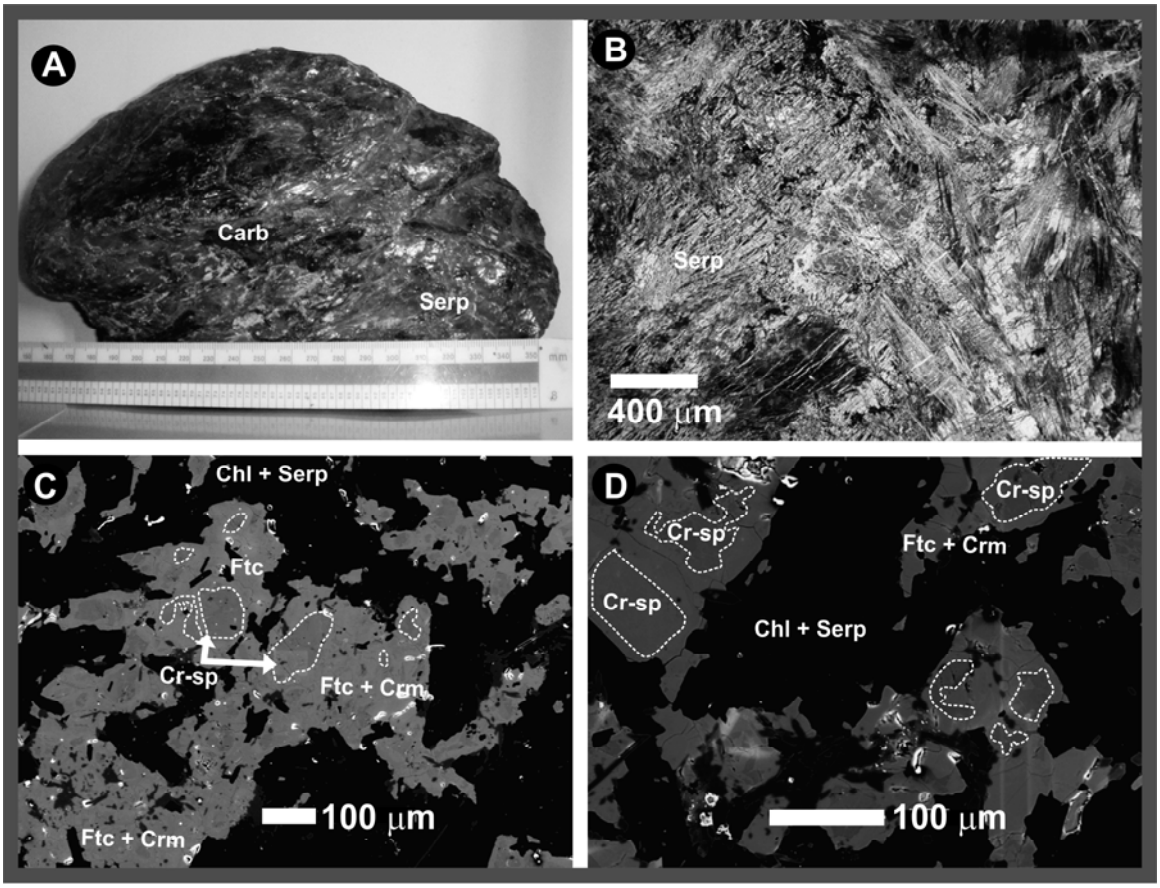

Figure 2. (a) Photomicrograph showing alteration of serpentinite and talc–carbonate (b) Mesh texture, (c) and (d) BE-SEM illustrating typical zoning patterns of Cr-spinel from GDS.

Table 1. Representative EMA of Cr-spinel cores, ferritchromite and Cr-magnetite in GDS

	C1	C2	C4	C5	C6	C8	C9	C10	C11	C12	C15	C16	C18	C20	F1	F2	F4	F5	F7	F9
wt %	Cr-spinel														Ferritchromite					
SiO_2	0.13	0.12	0.15	0.11	0.14	0.15	0.11	0.20	0.60	0.56	0.16	0.12	0.12	0.11	0.74	1.52	0.06	0.14	0.05	0.04
TiO_2	0.16	0.13	0.13	0.12	0.18	0.14	0.12	0.29	0.26	0.27	0.15	0.11	0.10	0.13	0.38	0.36	0.46	0.36	0.37	0.45
Al_2O_3	20.84	17.51	17.58	17.02	15.02	13.78	12.21	10.71	11.21	12.47	15.88	17.02	18.25	18.73	5.73	5.68	5.40	5.87	6.74	4.58
Cr_2O_3	46.89	48.82	49.57	51.14	52.33	53.74	54.41	55.74	54.83	52.64	51.78	50.66	49.28	48.36	45.12	47.01	48.13	50.12	46.21	45.08
Fe_2O_3	3.65	4.94	4.82	3.87	4.81	4.52	6.14	3.33	3.78	5.70	4.11	3.94	4.07	4.23	22.32	17.38	18.97	16.70	20.53	23.98
FeO	13.10	15.35	12.58	13.30	13.04	13.55	12.52	16.15	14.18	11.99	13.23	14.42	13.81	14.28	9.50	13.00	14.77	14.00	11.96	11.27
MnO	0.47	0.50	0.48	0.50	0.47	0.57	0.41	0.77	0.71	0.74	0.53	0.54	0.48	0.47	0.65	0.61	0.61	0.60	0.56	0.58
MgO	14.29	12.48	14.28	13.75	13.79	13.19	13.81	10.73	12.47	14.02	13.66	12.99	13.54	13.28	15.54	13.84	11.57	12.16	13.51	13.67
CaO	0.03	0.04	0.05	0.05	0.03	0.09	0.01	0.26	0.24	0.25	0.04	0.06	0.02	0.02	0.00	0.02	0.03	0.02	0.00	0.00
Total	**99.56**	**99.89**	**99.64**	**99.86**	**99.81**	**99.73**	**99.73**	**98.17**	**98.29**	**98.64**	**99.53**	**99.85**	**99.67**	**99.61**	**99.99**	**99.42**	**99.99**	**99.96**	**99.93**	**99.65**
apfu	***Cations per of 4 oxygen atoms***																			
Si	0.004	0.004	0.005	0.003	0.004	0.005	0.004	0.007	0.020	0.018	0.005	0.004	0.004	0.003	0.024	0.050	0.002	0.005	0.002	0.001
Ti	0.004	0.003	0.003	0.003	0.004	0.003	0.003	0.007	0.007	0.006	0.004	0.003	0.002	0.003	0.009	0.009	0.012	0.009	0.009	0.011
Al	0.757	0.651	0.647	0.629	0.560	0.519	0.461	0.421	0.433	0.473	0.591	0.632	0.673	0.691	0.220	0.221	0.214	0.231	0.262	0.180
Cr	1.143	1.218	1.224	1.268	1.308	1.357	1.378	1.468	1.421	1.340	1.294	1.262	1.219	1.197	1.164	1.228	1.279	1.323	1.206	1.191
Fe^{3+}	0.085	0.117	0.113	0.091	0.114	0.109	0.148	0.083	0.093	0.138	0.098	0.093	0.096	0.100	0.548	0.432	0.480	0.419	0.510	0.603
Fe^{2+}	0.338	0.405	0.329	0.349	0.345	0.362	0.335	0.450	0.389	0.323	0.350	0.380	0.361	0.374	0.259	0.359	0.415	0.391	0.330	0.315
Mn	0.012	0.013	0.013	0.013	0.013	0.015	0.011	0.022	0.020	0.020	0.014	0.014	0.013	0.013	0.018	0.017	0.017	0.017	0.016	0.016
Mg	0.657	0.587	0.665	0.643	0.650	0.628	0.660	0.533	0.610	0.673	0.644	0.610	0.632	0.620	0.756	0.682	0.580	0.605	0.665	0.681
Ca	0.001	0.001	0.002	0.002	0.001	0.003	0.000	0.009	0.008	0.009	0.001	0.002	0.001	0.001	0.000	0.001	0.001	0.001	0.000	0.000
Mg	0.66	0.59	0.67	0.65	0.65	0.63	0.66	0.54	0.61	0.68	0.65	0.62	0.64	0.62	0.74	0.65	0.58	0.61	0.67	0.68
Cr	0.60	0.65	0.65	0.67	0.70	0.72	0.75	0.78	0.77	0.74	0.69	0.67	0.64	0.63	0.84	0.85	0.86	0.85	0.82	0.87
Fe^{2+}	0.34	0.41	0.33	0.35	0.35	0.37	0.34	0.46	0.39	0.32	0.35	0.38	0.36	0.38	0.26	0.34	0.42	0.39	0.33	0.32
Fe^{3+}	0.04	0.06	0.06	0.05	0.06	0.05	0.07	0.04	0.05	0.07	0.05	0.05	0.05	0.05	0.28	0.23	0.24	0.21	0.26	0.31
Cr/Fe^{2+}	3.38	3.01	3.72	3.63	3.79	3.75	4.11	3.26	3.65	4.15	3.70	3.32	3.38	3.20	4.49	3.42	3.08	3.38	3.65	3.78
Al_2O_{3liq}	14.02	13.04	13.06	12.89	12.24	11.81	11.24	10.65	10.85	11.34	12.53	12.89	13.27	13.41						
FeO/MgO_{liq}	1.19	0.95	1.33	1.21	1.30	1.22	1.44	0.87	1.14	1.51	1.24	1.06	1.13	1.06						
F	19	20	20	20	20	21	21	22	21	21	20	20	20	19						

$Mg = Mg/(Mg+Fe^{2+})$, $Cr = Cr/(Cr+Al)$, $Fe^{3+} = Fe^{3+}/(Fe^{3+}+Cr+Al)$, $Fe^{2+} = Fe^{2+}/(Fe^{2+}+Mg)$, $(Al_2O_3)_{spinel}$ (wt %) $= 0.035(Al_2O_3)^{2.42}_{liquid}$ (wt %)
$ln(FeO/MgO)_{spinel} = 0.47 - 1.07Y^{Al}_{spinel} + 0.64Y^{Fe3+}_{spinel} + ln\ (FeO/MgO)_{liquid}$, $F = 10ln\ (Cr) + 24$

Table 1, continued

	F14	F15	F16	F17	F18	F20	F21	M1	M3	M5	M6	M7	M8	M9	M14	M22	M24	M25	M27	M28
wt %	Ferritchromite							Cr-magnetite												
SiO_2	0.15	0.12	0.41	0.17	0.05	0.23	0.31	0.24	0.27	0.24	0.15	0.27	0.75	1.89	0.51	0.37	0.59	0.33	0.43	0.41
TiO_2	0.40	0.41	0.25	0.26	0.41	0.37	0.28	0.45	0.41	0.27	0.42	0.27	0.37	0.27	0.39	0.26	0.26	0.24	0.25	0.24
Al_2O_3	6.01	5.73	7.21	6.24	5.84	6.42	5.71	0.26	0.29	0.16	0.30	0.19	0.22	0.24	0.42	0.20	0.20	0.17	0.18	0.19
Cr_2O_3	48.01	48.10	45.21	46.11	46.28	46.19	48.02	2.61	3.45	3.12	5.00	7.79	12.36	17.24	15.01	13.27	12.55	4.38	2.65	1.60
Fe_2O_3	18.72	19.34	20.13	21.35	20.90	20.14	19.20	63.65	61.55	63.18	60.18	58.26	53.29	46.94	50.76	52.78	53.04	61.35	63.21	64.02
FeO	13.01	12.74	12.44	11.36	13.47	12.50	12.89	29.85	29.13	27.61	28.96	27.10	26.33	24.61	26.34	27.35	27.51	28.31	27.39	28.56
MnO	0.62	0.54	0.58	0.62	0.61	0.62	0.63	0.55	0.59	0.44	0.61	0.64	0.50	1.05	0.53	0.51	0.50	0.41	0.39	0.37
MgO	12.78	13.02	13.41	13.85	12.43	13.18	12.94	0.34	0.40	1.51	0.40	1.74	2.96	4.73	2.78	1.87	1.96	1.13	1.80	1.05
CaO	0.01	0.00	0.00	0.00	0.00	0.01	0.01	0.33	0.37	0.24	0.38	0.25	0.24	0.26	0.25	0.24	0.24	0.22	0.23	0.23
Total	**99.70**	**100.0**	**99.65**	**99.96**	**99.99**	**99.66**	**99.98**	**98.27**	**96.47**	**96.77**	**96.40**	**96.51**	**97.03**	**97.23**	**96.99**	**96.83**	**96.85**	**96.54**	**96.51**	**96.68**
apfu	***Cations per of 4 oxygen atoms***																			
Si	0.005	0.004	0.014	0.006	0.002	0.008	0.010	0.009	0.011	0.009	0.006	0.011	0.029	0.071	0.020	0.014	0.023	0.013	0.017	0.016
Ti	0.010	0.010	0.006	0.006	0.010	0.009	0.007	0.013	0.012	0.008	0.013	0.008	0.011	0.008	0.011	0.008	0.008	0.007	0.007	0.007
Al	0.236	0.224	0.281	0.243	0.230	0.251	0.224	0.012	0.014	0.008	0.014	0.009	0.010	0.011	0.019	0.009	0.009	0.008	0.008	0.009
Cr	1.265	1.264	1.180	1.203	1.221	1.212	1.262	0.080	0.108	0.097	0.157	0.241	0.375	0.510	0.455	0.407	0.384	0.136	0.082	0.050
Fe^{3+}	0.469	0.484	0.500	0.530	0.525	0.503	0.480	1.863	1.833	1.862	1.792	1.713	1.537	1.323	1.465	1.540	1.546	1.816	1.862	1.895
Fe^{2+}	0.362	0.354	0.344	0.313	0.376	0.347	0.358	0.971	0.964	0.904	0.958	0.886	0.844	0.770	0.845	0.887	0.891	0.931	0.897	0.939
Mn	0.018	0.015	0.016	0.017	0.017	0.017	0.018	0.018	0.020	0.015	0.021	0.021	0.016	0.033	0.017	0.017	0.016	0.014	0.013	0.013
Mg	0.635	0.645	0.660	0.681	0.619	0.652	0.641	0.020	0.023	0.088	0.024	0.102	0.169	0.264	0.159	0.108	0.113	0.066	0.105	0.062
Ca	0.000	0.000	0.000	0.000	0.000	0.000	0.000	0.014	0.016	0.010	0.016	0.011	0.010	0.010	0.010	0.010	0.010	0.009	0.009	0.010
Mg	0.64	0.65	0.66	0.69	0.62	0.65	0.64	0.02	0.02	0.09	0.02	0.10	0.17	0.26	0.16	0.11	0.11	0.07	0.10	0.06
Cr	0.84	0.85	0.81	0.83	0.84	0.83	0.85	0.87	0.89	0.93	0.92	0.97	0.97	0.98	0.96	0.98	0.98	0.95	0.91	0.85
Fe^{2+}	0.36	0.35	0.34	0.31	0.38	0.35	0.36	0.98	0.98	0.91	0.98	0.9	0.83	0.74	0.84	0.89	0.89	0.93	0.9	0.94
Fe^{3+}	0.24	0.25	0.26	0.27	0.27	0.26	0.24	0.95	0.94	0.95	0.91	0.87	0.80	0.72	0.76	0.79	0.80	0.93	0.95	0.97
Cr/Fe^{2+}	3.49	3.57	3.43	3.84	3.25	3.49	3.53	0.08	0.11	0.11	0.16	0.27	0.44	0.66	0.54	0.46	0.43	0.15	0.09	0.05

Table 2. Representative EMA of serpentine in GDS

wt %	S1	S2	S3	S4	S5	S6	S7	S8	S9	S10	S11	S12	S13	S14	S15	S16	S17	S18	S19	S20
SiO_2	43.98	44.72	44.14	45.02	44.68	44.37	44.62	44.27	43.81	43.91	43.16	43.62	44.08	43.71	44.76	43.47	44.17	44.38	44.28	43.69
TiO_2	0.00	0.02	0.02	0.01	0.01	0.02	0.01	0.02	0.03	0.03	0.02	0.01	0.01	0.02	0.01	0.02	0.01	0.03	0.01	0.02
Al_2O_3	1.22	0.91	1.68	1.88	1.57	0.99	0.43	1.22	0.99	1.01	0.93	1.49	1.09	1.28	1.25	1.33	1.02	1.08	0.69	2.04
Cr_2O_3	1.18	0.54	0.55	0.32	0.48	0.45	0.05	0.18	0.39	0.25	0.04	0.85	0.61	0.25	0.46	0.17	0.44	0.14	0.18	0.44
FeO_{total}	2.11	2.16	2.40	2.81	1.99	1.23	1.08	2.05	0.92	1.60	2.88	2.97	2.57	2.55	1.22	1.55	1.35	1.68	1.33	2.67
MnO	0.05	0.05	0.07	0.06	0.05	0.05	0.03	0.05	0.09	0.04	0.00	0.05	0.06	0.05	0.04	0.06	0.04	0.05	0.03	0.06
MgO	38.73	38.67	38.04	38.24	38.21	39.73	40.22	38.75	40.84	40.25	39.97	38.24	38.61	38.91	39.22	40.35	39.65	39.23	40.81	38.00
CaO	0.01	0.01	0.02	0.01	0.00	0.01	0.01	0.02	0.02	0.01	0.03	0.01	0.01	0.01	0.01	0.01	0.00	0.02	0.01	0.01
Na_2O	0.00	0.01	0.01	0.00	0.00	0.00	0.01	0.01	0.00	0.00	0.00	0.01	0.00	0.01	0.01	0.00	0.01	0.00	0.01	0.00
K_2O	0.00	0.00	0.00	0.00	0.01	0.01	0.00	0.01	0.02	0.02	0.01	0.00	0.00	0.00	0.00	0.00	0.01	0.01	0.01	0.01
Totals	**87.27**	**87.07**	**86.91**	**88.35**	**86.98**	**86.84**	**86.44**	**86.56**	**87.09**	**87.10**	**87.03**	**87.25**	**87.04**	**86.79**	**86.98**	**86.97**	**86.70**	**86.61**	**87.35**	**86.92**
apfu	***Cations per of 14 oxygen atoms***																			
Si	8.152	8.281	8.200	8.230	8.264	8.209	8.276	8.237	8.090	8.125	8.054	8.118	8.196	8.148	8.255	8.058	8.192	8.239	8.157	8.130
Ti	0.000	0.002	0.003	0.001	0.001	0.002	0.001	0.003	0.004	0.003	0.002	0.002	0.001	0.003	0.001	0.003	0.001	0.004	0.001	0.002
Al	0.267	0.199	0.368	0.404	0.343	0.215	0.093	0.268	0.214	0.219	0.205	0.327	0.239	0.281	0.272	0.291	0.223	0.236	0.150	0.447
Cr	0.172	0.078	0.081	0.046	0.070	0.065	0.007	0.026	0.057	0.036	0.006	0.126	0.090	0.037	0.067	0.024	0.065	0.020	0.026	0.065
Fe_{total}	0.326	0.334	0.372	0.430	0.307	0.191	0.167	0.319	0.143	0.247	0.449	0.462	0.400	0.398	0.189	0.240	0.209	0.261	0.205	0.416
Mn	0.008	0.007	0.010	0.009	0.007	0.008	0.004	0.007	0.013	0.006	0.000	0.008	0.009	0.007	0.007	0.009	0.007	0.007	0.004	0.009
Mg	10.70	10.67	10.53	10.42	10.53	10.95	11.12	10.74	11.24	11.10	11.11	10.60	10.70	10.81	10.78	11.15	10.96	10.85	11.21	10.54
Ca	0.001	0.001	0.003	0.002	0.000	0.001	0.001	0.003	0.003	0.002	0.005	0.001	0.001	0.001	0.001	0.003	0.000	0.004	0.002	0.001
Na	0.000	0.004	0.004	0.000	0.000	0.000	0.004	0.004	0.000	0.000	0.000	0.002	0.000	0.002	0.002	0.000	0.002	0.000	0.002	0.000
K	0.000	0.000	0.000	0.000	0.001	0.001	0.000	0.001	0.004	0.004	0.002	0.000	0.001	0.000	0.001	0.001	0.002	0.002	0.002	0.001
Mg	0.970	0.970	0.966	0.960	0.972	0.983	0.985	0.971	0.988	0.978	0.961	0.958	0.964	0.965	0.983	0.979	0.981	0.977	0.982	0.962

Mg = Mg/(Mg+Fe)

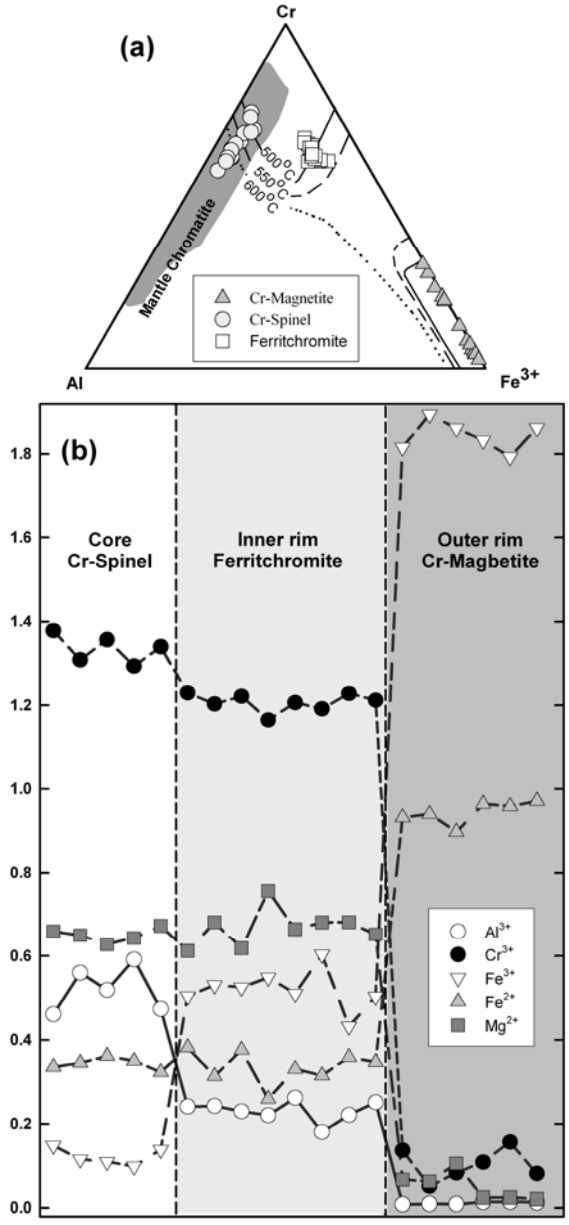

Figure 3. (a) Composition of investigated Cr-spinel cores and rims, stability limits after Sack & Ghiorso (1991) (b) Compositional variations of Cr^{3+}, Al^{3+}, Fe^{3+}, Fe^{2+} and Mg^{2+} (*apfu)*, through representative zoned Cr-spinel grains showing the alteration zones identified in the studied Cr-spinel.

4.2. Serpentine chemistry and Raman investigations

The principal minerals of the serpentine group, chrysotile, antigorite and lizardite, have a very similar composition, but significantly different structures. In fact, the single ideal chemical formula $[(OH)_3Mg_3[Si_2O_5(OH)]$ corresponds to several crystal structures that represent different solutions for the minimization of the mismatch between sheets of SiO_4 tetrahedra and sheets of $Mg_3O_2(OH)_4$ octahedra (Rinaudo et al., 2003).

Representative EMA of serpentine, from the investigated rocks are given in table 2. The analyzed serpentine contains low Al_2O_3 (0.43–2.04 wt%), whereas FeO ranges from 0.92 to 2.97 wt%. All the serpentine grains contain some Cr (0.04–1.18 wt% Cr_2O_3), presumably introduced from Cr-spinel during serpentinization. On the SiO_2 vs. MgO diagram of Dungan (1979), the investigated serpentine minerals plot in the field of antigorite (Fig. 4a).

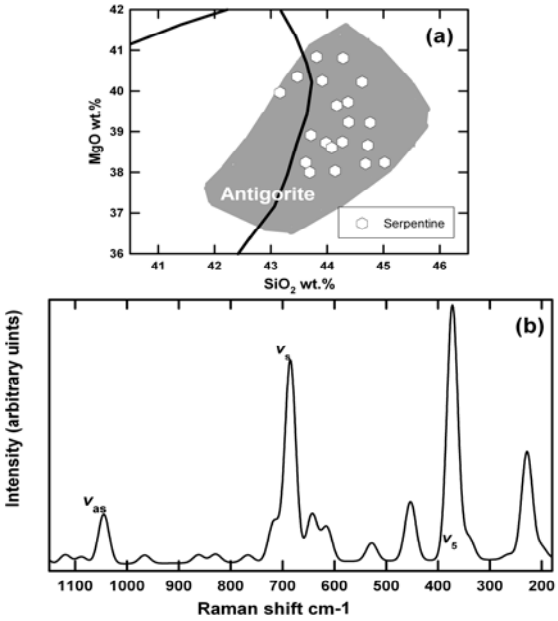

Figure 4. (a) Serpentine compositions plotted on SiO_2 vs. MgO diagram, (b) Raman spectra of antigorite

Due to their similar compositions, serpentine minerals are difficult to properly identify in the absence of X-ray data (Deer et al., 1992). Raman spectroscopy has been used successfully by a number of investigators in the study of chrysotile, antigorite and lizardite (Rinaudo et al., 2003). Antigorite is easily distinguished from the other two serpentine phases for the presence of a band at about 685 cm^{-1}, assigned to the Si-O_b-Si vibrations by Rinaudo et al., (2003). On the other hand, chrysotile and lizardite may be distinguished on the basis of the SiO_4 tetrahedra bending modes: in chrysotile they occur at 390 cm^{-1}, while in lizardite between 380 and 388 cm^{-1} (Groppo et al., 2006).

Figure 4b, show Raman spectra obtained on the antigorite sample. The main bands are assigned according to the assignment for antigorite as suggested by Rinaudo et al., (2003). The characteristic bands of antigorite from GDS are similar to the spectra of antigorite from Rinaudo et al., (2003). The band occurring at 1045 cm^{-1} is correspond to the band observed in the Raman spectrum of this mineral at 1044 cm^{-1} and ascribed

by Rinaudo et al., (2003) to antisymmetric stretching modes (v_{as}) of the Si–O_b–Si groups (E_1), whereas the intense band at 685 cm^{-1} produced by symmetric stretching modes (v_s) of the Si–O_b–Si linkages. The bands at 642 and 373 cm^{-1} ascribed by Rinaudo et al., (2003) to the OH–Mg–OH translation modes and to $v_5(E)$ modes of the SiO_4 tetrahedra, respectively. The bands at 229 and 529 cm^{-1} are assigned to the vibrations of the O–H–O groups and to the deformation modes of the SiO_4 tetrahedra, respectively (Rinaudo et al., 2003).

Based on the Raman spectra together with the SiO_2 vs. MgO diagram of Dungan (1979), it can be speculated that all the serpentines are antigorite.

4.3. Chlorite chemistry and thermometry

Representative EMA of chlorites is given in table 3. All the studied chlorites correspond to the tri-trioctahedral group, based on the Wiewióra & Weiss (1990) classification. The structural formulae (Table 3) were calculated on the basis of $O_{20}(OH)_{16}$. This is probably appropriate for metamorphic trioctahedral chlorite based on the study of Hillier & Velde (1991). The sum of octahedral cations is very close to 12 in all samples confirming that the chlorite is predominantly trioctahedral. The chlorite ranges from clinochlore to penninite based on the nomenclature of Hey (1954). In order to constrain the chlorite formation temperatures, chlorite thermometry based on the equation of Xie et al., (1997) was employed. The penninite apparently formed at lower temperatures (261 ± 25°C) than the clinochlore (351 ± 10°C).

4.4. Whole-Rock major and trace elements

Representative chemical analyses of GDS major and trace elements are given in table 4. Because of the GDS alteration and its lack of primary mineral phases, it was impossible to calculate the normative values. All samples contain abundant water, with LOI ranging from 11.50% to 11.80 %, averaging 11.65 %. Mean compositions of GDS are SiO_2 = 40.00 ± 0.47 wt%, MgO = 37.64 ± 0.11 wt%, Al_2O_3 = 1.90 ± 0.13wt% and CaO = 0.21 ± 0.06 wt%. This is a relatively restricted range and suggests that elemental redistribution associated with serpentinization was limited. Ca metasomatism is a common concern in Egyptian serpentinites because of pervasive carbonate alteration (Stern & Gwinn 1990), but the low and restricted range of CaO in the GDS suggests that this was limited in the samples we have analyzed.

The REE patterns of GDS are characterized by LREE-HREE profiles with positive slopes (Fig. 5a). A characteristic feature of REE patterns is the negative Ce anomaly, which probably results from the mobility of the trivalent LREE during secondary alteration (e. g. Gruau et al., 1998), such as, seafloor weathering or serpentinization (Niu, 2004).

Table 3. Representative EMA of chlorite in GDS

	H1	H2	H3	H4	H5	H6	H7	H8	H9	H11	H14
wt %	**Penninite**						**Clinochlore**				
SiO_2	35.22	33.25	33.58	34.25	33.61	34.28	32.11	31.55	32.05	31.21	30.55
TiO_2	0.03	0.02	0.06	0.02	0.03	0.02	0.09	0.03	0.03	0.03	0.02
Al_2O_3	9.87	12.45	11.81	11.02	12.86	11.25	14.54	15.22	15.52	16.95	16.58
FeO_{total}	5.84	6.25	4.97	7.25	4.62	6.54	3.60	4.85	2.51	4.84	5.74
MnO	0.02	0.02	0.02	0.01	0.03	0.01	0.03	0.01	0.03	0.02	0.01
MgO	33.97	33.05	33.75	32.47	34.01	33.14	33.05	32.25	34.55	32.11	31.02
Cr_2O_3	2.26	1.96	3.05	2.26	2.14	2.24	3.37	2.50	2.51	1.75	0.41
Total	**87.2**	**87.01**	**87.25**	**87.28**	**87.30**	**87.48**	**86.78**	**86.41**	**87.19**	**86.91**	**84.33**
apfu	***Cations per of $O_{20}(OH)_{16}$***										
Si	6.743	6.396	6.429	6.602	6.396	6.571	6.138	6.084	6.051	5.966	6.022
Al^{iv}	1.257	1.604	1.571	1.398	1.604	1.429	1.862	1.916	1.949	2.034	1.978
IV site	**8.00**	**8.00**	**8.00**	**8.00**	**8.00**	**8.00**	**8.00**	**8.00**	**8.00**	**8.00**	**8.00**
Al^{vi}	0.972	1.223	1.095	1.107	1.281	1.114	1.417	1.545	1.507	1.787	1.876
Ti	0.004	0.003	0.009	0.003	0.004	0.003	0.012	0.004	0.004	0.004	0.003
Cr	0.342	0.299	0.461	0.345	0.322	0.340	0.509	0.382	0.374	0.265	0.065
Fe_{total}	0.935	1.036	0.796	1.169	0.735	1.049	0.575	0.782	0.422	0.774	0.959
Mn	0.002	0.004	0.004	0.002	0.005	0.002	0.005	0.002	0.005	0.003	0.002
Mg	9.695	9.478	9.632	9.330	9.648	9.470	9.417	9.271	9.723	9.150	9.115
Vacancy	0.050	0.00	0.003	0.044	0.005	0.022	0.065	0.014	0.00	0.017	0.00
VI site	**12.00**	**12.04**	**12.00**	**12.00**	**12.00**	**12.00**	**12.00**	**12.00**	**12.04**	**12.00**	**12.02**
Fe/Fe+Mg	**0.088**	**0.099**	**0.076**	**0.111**	**0.071**	**0.100**	**0.058**	**0.078**	**0.042**	**0.078**	**0.095**
T	**235**	**287**	**291**	**248**	**299**	**258**	**346**	**346**	**367**	**365**	**349**

$T = 321.98[Al^{IV} + 1.33\ (0.31 – (Fe/Fe + Mg))] – 61.92$ when $Fe/Fe + Mg < 0.31$, (Xie et al., 1997)

The compositions of GDS indicate the enrichment of fluid mobile elements (As, Sb, Pb, Sr; Fig. 5b). Figure 5b shows the distribution of lithophile trace elements normalized to primitive upper mantle (Sun & McDonough, 1989) for the GDS. They are depleted in terms of lithophile trace elements. Nevertheless, they show variable relative enrichment in the most of incompatible trace elements (Cs, U, and Nb), and exhibit a positive Sr spike.

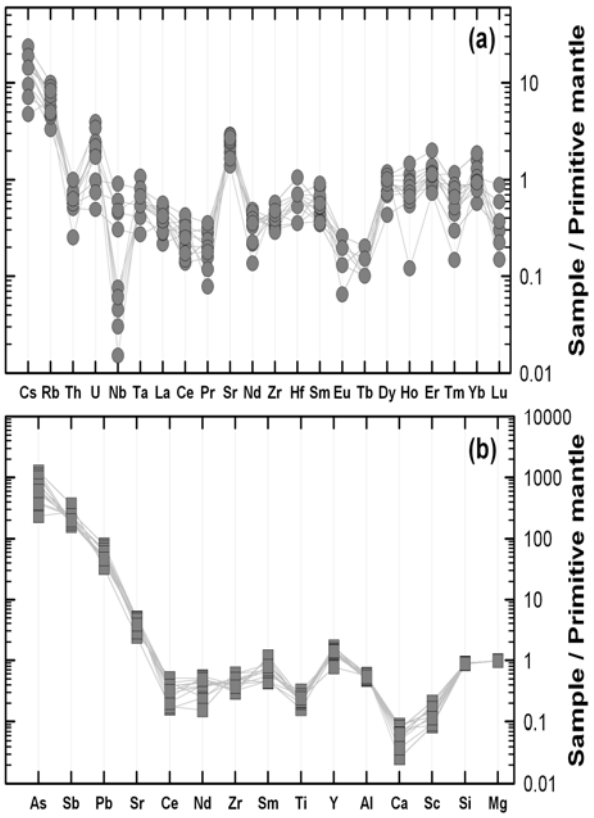

Figure 5. (a) GDS normalized REE patterns and (b) trace element spidergram normalized to primitive mantle of Sun & McDonough (1989).

5. DISCUSSIONS

5.1. Cr-spinel composition of GDS

Actually, three different spinel compositions have been distinguished within the GDS: i.e, magmatic Cr-spinels (core) and metamorphic ferritchromit (intermediate zone) and Cr-magnetite (outer rim). Each of these spinels conveys information about different steps of the serpentinites evolution, as hence after reported in detail.

It has been evident from figure 3a together with the high and restricted ranges of Cr (0.60-0.78) and Mg (0.54-0.68) in the magmatic Cr-spinels cores (Table 1) that their primary compositions are not affected by metamorphism. So, they can be used as petrogenetic indicator.

Many researchers have proposed that diffusion of Al and Mg out of the Cr-spinel during metamorphism results in the formation of chlorite (Shen et al., 1988) or chlorite together with ferritchromite (Wylie et al., 1987; Kimball, 1990; Merlini et al., 2009). The formation of ferritchromite and chlorite can be explained using the following reactions proposed by Kimball (1990) and Merlini et al., (2009):

$$(Mg,Fe)(Al,Cr)_2O_4 + Fluid \rightarrow$$
Cr–spinel

$$Mg_5AlSi_3AlO_{10}(OH)_8 + Fe(FeCr)_2O_4 \quad \textbf{(I)}$$
chlorite *Ferritchromite*

$$2(Mg,Fe)(Al,Cr)_2O_4 + 3/2Mg_3Si_2O_5(OH)_4 + H_2O$$
Cr–spinel *serpentine*

$$+ 1/12O_2$$

$$\rightarrow 1/2(MgAl)_{12}(Al_2Si_6)O_{20}(OH) + 7/6Fe(FeCr)_2O_4 \quad \textbf{(II)}$$
chlorite *Ferritchromite*

The breakdown of spinel to form chlorite through these reactions implies outward diffusion of Al and Mg from Cr- spinel, leaving a residual Fe^{3+}-enriched and Al-, Mg-depleted Cr-spinel (ferritchromite). The formation of ferritchromite and chlorite through these reactions took place at relatively high temperatures (> 400ºC) Kimball (1990), and in the presence of aqueous fluids (Merlini et al., 2009).

The temperatures proposed by (Kimball, 1990) indicates that this alteration event do not concur with those at which greenschist facies metamorphism is often commenced (200-400ºC; Früh-Green et al., 2001; Bach et al., 2010). However, the combined serpentinization of olivine and pyroxene (Bach et al., 2006) at lower temperatures (200-300ºC) could favor the creation of an aqueous fluid rich environment necessary for the reactions I and II to take place.

The Cr-magnetite is either formed as part of some continuous process that began with ferritchromit and ended with Cr-magnetite (Wylie et al., 1987), or is the product of fluid-driven reaction between Cr-spinel and surrounding chlorite (Barnes, 2000). Nevertheless, the progressive Fe^{3+} enrichment from core to rim in the studied Cr-spinel (Fig. 3b) suggests a change in the alteration conditions to more oxidative states with increasing metamorphism.

At relatively high oxidative conditions, favor the reaction of spinel with serpentine to produce chlorite and Cr-magnetite according to Mellini et al., (2005):

$$(Mg,Fe)(Al,Cr)_2O_4 + 1.5Mg_3Si_2O_5(OH)_4 + H_2O$$
Cr–spinel *serpentine*

$$+ 0.083O_2$$

$$\rightarrow Mg_5AlSi_3AlO_{10}(OH)_8 + 0.167\ (Fe,Cr)_3O_4 \quad \textbf{(III)}$$
chlorite *Cr – magnetite*

Table 4. Representative whole rock major elements and compositions of REEs and trace elements of GDS

wt %	R1	R2	R3	R4	R5	R6	R7	R8	R9	R10	R11
SiO_2	39.83	39.28	39.86	41.00	39.38	40.31	39.97	39.88	40.58	39.89	39.90
TiO_2	0.03	0.02	0.03	0.04	0.03	0.03	0.03	0.03	0.03	0.03	0.03
Al_2O_3	1.86	1.74	1.97	1.95	2.13	1.69	1.99	2.06	1.78	1.81	1.92
Fe_2O_3	8.26	8.11	7.07	5.15	8.18	7.15	6.11	7.48	6.16	6.80	7.18
FeO_l	1.71	2.03	2.39	2.60	2.35	1.75	2.88	2.27	2.20	2.38	2.29
MgO	37.48	37.67	37.87	37.59	37.77	37.57	37.69	37.77	37.52	37.58	37.58
MnO	0.10	0.10	0.12	0.13	0.11	0.11	0.12	0.11	0.12	0.11	0.11
CaO	0.17	0.21	0.17	0.29	0.09	0.25	0.25	0.12	0.29	0.26	0.21
Na^2O	0.03	0.02	0.03	0.03	0.03	0.03	0.03	0.03	0.03	0.02	0.03
K_2O	0.01	0.01	0.01	0.00	0.01	0.01	0.01	0.01	0.00	0.01	0.01
P_2O_5	0.01	0.02	0.03	0.03	0.02	0.02	0.03	0.02	0.02	0.02	0.02
Total	**89.46**	**89.19**	**89.51**	**88.80**	**90.06**	**88.90**	**89.08**	**89.78**	**88.72**	**88.91**	**89.27**
LOI	11.80	11.78	11.50	11.55	11.52	11.78	11.55	11.51	11.72	11.72	11.67
ppm											
Sc	2.1	1.8	3.1	2.3	1.4	3.4	1.4	1.5	2	2.5	2.7
As	40.2	62.1	11.8	27.2	33.4	18.6	62.7	55.4	51.2	36.9	19.5
Rb	3.0	6.0	4.0	2.0	3.4	5.4	4.0	2.9	4.5	5.0	3.0
Sr	44	58	57	51	38	49	28	33	51	57	54
Y	5.2	4.8	6.0	4.3	5.8	6.1	2.8	4.7	5.0	5.4	5.1
Zr	5.0	3.2	6.0	4.0	3.5	4.8	6.1	3.0	4.1	4.6	5.0
Nb	0.40	0.20	0.60	0.03	0.05	0.04	0.02	0.01	0.30	0.40	0.31
Sb	1.0	1.0	1.5	1.2	1.0	1.3	2.0	0.9	1.0	1.2	1.3
Cs	0.3	0.5	0.1	0.2	0.4	0.3	0.4	0.2	0.4	0.3	0.1
Ba	6	4	3	5	2	4	3	1	5	3	4
La	0.14	0.23	0.26	0.28	0.34	0.18	0.26	0.37	0.18	0.24	0.27
Hf	0.20	0.10	0.20	0.20	0.10	0.10	0.30	0.20	0.15	0.15	0.20
Ta	0.020	0.015	0.030	0.020	0.020	0.040	0.020	0.030	0.015	0.020	0.025
Pb	7.0	8.0	12.0	6.0	8.0	7.0	5.0	11.0	7.5	10.0	9.0
Th	0.06	0.04	0.05	0.05	0.06	0.05	0.08	0.02	0.05	0.04	0.05
U	0.08	0.01	0.02	0.05	0.04	0.05	0.07	0.05	0.04	0.01	0.03
Ce	0.47	0.61	0.23	0.35	0.54	0.61	0.25	0.71	0.54	0.42	0.29
Pr	0.080	0.020	0.040	0.050	0.070	0.020	0.060	0.090	0.050	0.030	0.045
Nd	0.42	0.55	0.27	0.61	0.47	0.28	0.17	0.57	0.48	0.41	0.44
Sm	0.14	0.15	0.28	0.18	0.34	0.21	0.22	0.37	0.14	0.21	0.23
Eu	0.02	0.04	0.02	0.04	0.04	0.03	0.02	0.01	0.03	0.03	0.03
Tb	0.02	0.01	0.01	0.02	0.02	0.01	0.01	0.02	0.01	0.01	0.01
Dy	0.47	0.51	0.73	0.63	0.73	0.29	0.81	0.74	0.49	0.62	0.68
Ho	0.11	0.14	0.08	0.12	0.17	0.09	0.02	0.22	0.12	0.11	0.10
Er	0.37	0.61	0.42	0.58	0.61	0.49	0.32	0.88	0.49	0.51	0.50
Tm	0.02	0.05	0.06	0.03	0.03	0.08	0.01	0.06	0.03	0.05	0.04
Yb	0.25	0.45	0.39	0.44	0.71	0.83	0.47	0.40	0.35	0.42	0.41
Lu	0.02	0.01	0.04	0.01	0.02	0.01	0.06	0.02	0.01	0.02	0.02

Reaction III is mainly controlled by $f(O_2)$ in the environment. The progressive increase of $f(O_2)$ favored the reaction of higher amounts of serpentine and Cr-spinel, producing Cr-magnetite and chlorite which, found as inclusions at Cr-magnetite alteration margins or forming haloes around Cr-spinel. The $f(O_2)$ increase required for the formation of Cr-magnetite may be took place after the late stages of serpentinization or during lower temperature amphibolite facies metamorphism (Bach et al., 2006).

Cr-spinel is the favorable receptor for Mn, most probably during serpentinization process in the absence of ilmenite and garnet, (Deer et al., 1992). The investigated spinels (core and rim) contain very low MnO. Barnes (2000) attributed the decrease of Mn in the Cr-spinels to the presence of carbonate. The scarce proportion of magnesite in the studied GDS, suggests a late, highly oxidizing conditions accompanied by limited influence of CO_2-rich fluids (Barnes, 2000).

5.2. Grade of metamorphism

One of the fundamental problems related to the study of serpentinites is the determination of their metamorphic grade. In the absence of olivine or pyroxene, there is neither reliable geothermometer nor geobarometer which can be applied to these rocks. Thus, the Cr-spinel composition becomes an important tool for determining the metamorphic grade (Abzalov, 1998).

The above described Cr-spinel alteration reflects that ferritchromits and /or Cr-magnetite have been formed around the transitional greenschist–amphibolite facies to lower amphibolite facies metamorphism. Moreover, figure 3a shows that (1) a miscibility gap exists between Cr-spinels core and rims corresponding to metamorphism around ~500-600°C and (2) no complete solid solution exists between ferritchromit and Cr-magnetite.

The miscibility gap between Cr-spinels core and rims reflects the incomplete re-equilibration between the Cr-spinels core and rims in lowest amphibolite facies (i.e. around ~500- 600°C). Barnes (2000) concluded that Cr-spinel, which equilibrated in lowest amphibolite facies rocks, retains their original igneous chemical composition. However, Mg values are substantially lowered by Fe–Mg exchange with silicates and/or carbonates. The investigated ferritchromits preserve high Cr-contents (45.12 - 50.12 wt%) close to those of the magmatic cores (46.89 – 55.74 wt%), but apparently low Fe^{2+} (0.26 – 0.42), indicating the formation of ferritchromits took place during the lower amphibolite facies.

Furthermore, the absence of a complete solid solution between ferritchromit and Cr-magnetite or the occurrence of a compositional gap between them indicates also their formation during the lower amphibolite facies. Thus this compositional gap widens rapidly below 550°C (Barnes, 2000) and there is a complete solid solution from Cr-spinels to magnetite above 600°C (Sack & Ghiorso, 1991). In addition, Mg for ferritchromits and Cr-magnetite varies from 0.58 to 0.74 and from 0.01 to 0.26, respectively, which coincide with those of the transitional greenschist–amphibolite facies metamorphism suggested by Barnes (2000).

Furthermore, the preservation of antigorite grains as the only serpentine mineral, together with the absence of newly formed olivine can be considered as further evidence. Thus the antigorite formation took place at ~ 500°C (Moody, 1976), whereas the olivine forms after antigorite by dehydration at > 500ºC; (Caruso & Chernosky, 1979), which is the minimum temperature for the formation of ferritchromit, antigorite, and chlorite (Jan & Windley, 1990). The former observation suggests also that the temperature did not exceed the range of lower amphibolite facies metamorphism. Another evidence can be obtained from the chlorite geothermometry, which suggests that serpentinization-chloritization processes occurred at 250° to 400°C.

Winter (2001) stated that in orogenic belts, ultramafic bodies are commonly metamorphosed to the same grade as the surrounding rocks. According to Akaad & El-Ela (1996), the surrounding rocks (metagabbros and metavolcanics) of GDS have been overprinted by a greenschist to low grade amphibolite facies metamorphism. Moreover, the transitional greenschist-amphibolite facies was prevailing during the metamorphic evolution of the Pan-African belt of Egypt (Abu El Elaa & Farahat, 2010).

The described evolution of the alteration process shows that alteration rims in metamorphosed Cr-spinel are a faithful record of the metamorphic path. The low temperature serpentinization, occurring during the lower- to mid-greenschist facies metamorphism most probably did not produce any change in Cr-spinel composition as it took place under highly reducing conditions (Bach et al., 2006). The replacement of primary Cr-spinel rims by ferritchromite and Cr-magnetite likely takes place after the main-stage serpentinization. Prograde metamorphism stops the serpentinization of olivine and pyroxene, promoting the creation of a relatively more oxidizing environment (Bach et al., 2006). With the increasing temperature, during the late stages of greenschist facies metamorphism or around the transitional greenschist-amphibolite to lower amphibolite facies, Cr-spinel reacts with serpentine in the presence of aqueous fluids, giving rise to a new Cr-spinel rich in Fe_2O_3 and Cr_2O_3 (i.e. ferritchromit) in equilibrium with chlorite. Then, under more oxidizing conditions, higher amounts of serpentine react with the pre-existing Cr-spinel (both altered and unaltered), producing a new alteration rim (i.e. Cr-magnetite) characterized by higher Fe^{3+} content and an abundance of chlorite. At the end of the evolutionary history of GDS, serpentine reacted with Cr-magnetite to form carbonates (magnesite) in the silicate matrix of GDS or along late narrow veins.

5.3. Petrogenetic and geotectonic evolution

Arai & Yurimoto (1994) mentioned that the Cr of the spinel in harzburgite (~ 0.5) is lower than those of dunite (~0.7). The Cr of the investigated spinel cores varies from 0.60 to 0.78, reflecting variation in the parent peridotites from harzburgite to dunite. Furthermore the whole rock major

elements (Table 4) plotted in a Al_2O_3-CaO-MgO ternary diagram (Fig. 6a) show that the GDS correspond to a harzburgitic protolith.

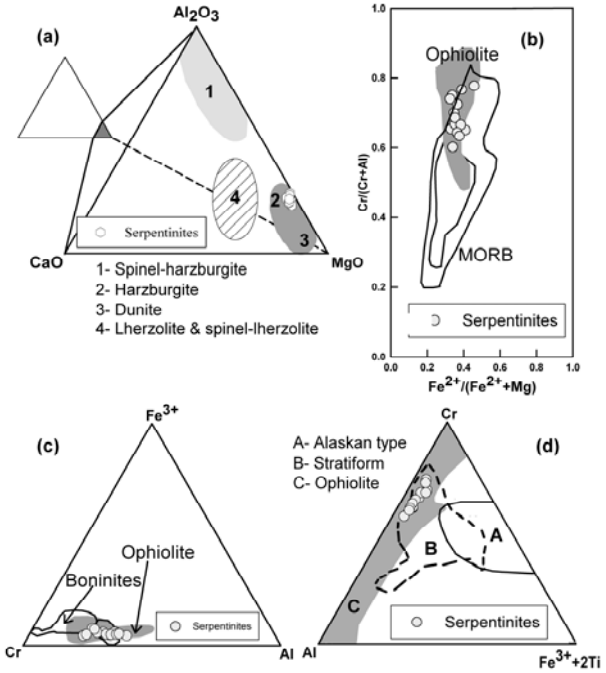

Figure 6. (a) Relationship between serpentinites and their protoliths in a MgO-Al_2O_3-CaO (wt%) ternary diagram (fields from Li et al., 2004) and Cr-spinel core compositions plotted on (b) Cr–Al–Fe^{3+}, (c) $Fe^{2+}/(Mg+Fe^{2+})$ vs. Cr/(Cr+Al) (Barnes & Roeder, 2001), and (d) Al–Cr–(Fe^{3+}+2Ti) (Jan & Windley, 1990).

Figure 6b, c and d together with the very low TiO_2 contents (0.10–0.29 wt%) of the Cr-spinel cores are typical to those from ophiolitic rocks of depleted mantle source. Jan & Windley (1990) suggested a TiO_2 level of 0.3 wt% as the dividing boundary between Cr-spinels from ophiolite of depleted mantle source and those from other complexes, which generally contain > 0.3 wt% TiO_2. Barnes & Roeder (2001) demonstrated that the parent magma of ophiolitic cumulates formed from high degrees of melting of reduced and depleted mantle, which is clearly the case of the investigated GDS. Moreover, the high Cr/Al ratios of the investigated spinel cores (Cr = 0.60 - 0.78) points to higher degree of partial melting of depleted mantle source (Bonatti & Michael, 1989). In addition, the degree of partial melting (F) of the GDS, calculated on the base of the empirical equation proposed by Hellebrand et al., (2001), $F = 10\ ln\ (Cr) + 24$, suggests partial melting up to 22% (Table 1).

Further insights into the chemistry of the parental melts for the studied GDS can be gained using the following equations of Maurel & Maurel (1982):

$$(Al_2O_3)_{spinel}\ (wt\ \%) = 0.035(Al_2O_3)^{2.42}_{liquid}\ (wt\ \%)$$

$$ln(FeO/MgO)_{spinel} = 0.47 - 1.07Y^{Al}_{spinel} + 0.64Y^{Fe3+}_{spinel} + ln\ (FeO/MgO)_{liquid}$$

FeO and MgO in wt% and

$Y^{Al}_{spinel} = Al/(Al+Cr+Fe^{3+})$

$Y^{Fe3+}_{spinel} = Fe^{3+}/(Al+Cr+Fe^{3+})$

The results show that melts had an average Al_2O_3 content of 12.37 wt% (10.65–14.20 wt%) and FeO/MgO between 0.87 and 1.19 (Table 1). These values compare with those of the low-Ti, high-Mg tholeiitic [Al_2O_3 = 11.40–16.40 wt%, (Augé, 1987)], and boninitic [Al_2O_3 = 10.60–14.40 wt%, FeO/MgO = 0.70 – 1.40, (Wilson, 1989)] primary magmas.

The likely low-Ti tholeiitic to boninitic affinity of the GDS parental melt suggests formation in an arc–marginal basin setting. Consistently, the geochemistry of the associated metavolcanics points to an island arc tholeiitic affinity (Akaad & El-Ela, 1996). In addition, arc tholeiitic to boninitic affinities have been suggested for some ophiolitic metavolcanics and metagabbros from the central Eastern Desert of Egypt (Farahat, 2001).

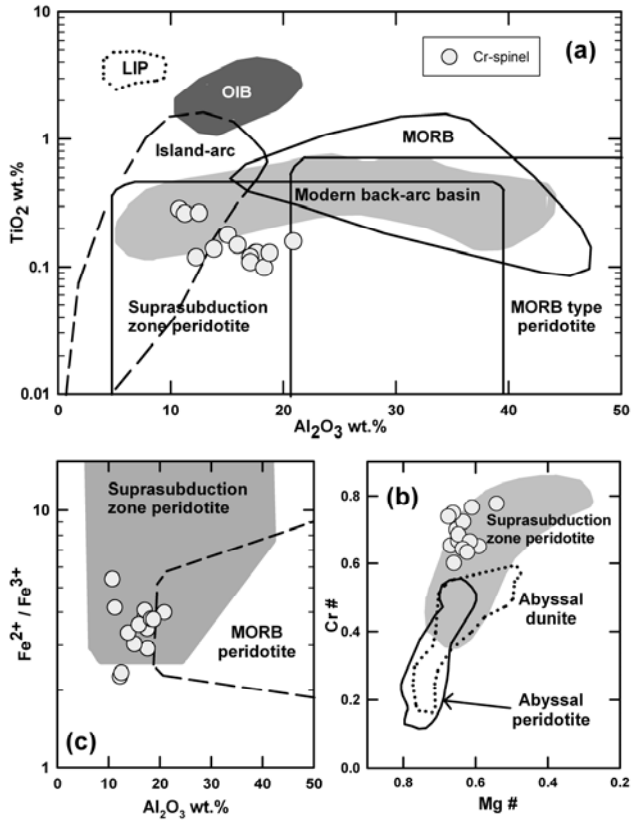

Figure 7. Cr-spinel core compositions plotted on (a) TiO_2 vs. Al_2O_3, (b) Mg# vs. Cr# and (c) Al_2O_3 vs. Fe^{2+}/Fe^{3+} tectonic discrimination diagrams.

On the Al_2O_3 vs. TiO_2, Mg vs. Cr and Al_2O_3 vs. Fe^{2+}/Fe^{3+} diagrams (Fig. 7) of Kamenetsky et al., (2001) the investigated Cr-spinel cores clearly plot

in the suprasubduction zones (SSZ) peridotites (i.e. marginal basin). Furthermore, the degree of partial melting (*F*) of the GDS (*F* = 19-22 %, Table 1) is within the range of peridotites from SSZ [*F* = 15-40, (Mellini et al., 2005)]. Moreover preliminary REE geochemistry of GDS displays morphological REE patterns with flat to negative slope trends (Fig. 5a). These patterns are more characteristic of SSZ and may be due to secondary metasomatism during subduction or metamorphic interaction with the continental crust. The extremely low content of tantalum in the GDS and low content of thorium (Table 4), compared to ytterbium also indicates a suprasubduction environment (Gorton & Schandl, 2000), probably associated with an oceanic arc.

Furthermore, the Egyptian ophiolities have a strong geochemical affinity to marginal basin tectonic settings (Farahat et al., 2004; El Gaby, 2005). Farahat et al., (2004) studied the geochemical characteristics of many ophiolities from the central part of the ED of Egypt and concluded that Egyptian ophiolities are all of marginal basins origin and none of them show a true MORB affinity. Moreover, the age of the ophiolites from the ED of Egypt is a little older than the age of the associated island arc volcanics, implying that they have been formed in a region close to their acceleration such as marginal basins rather than in a remote mid-ocean spreading-ridge regime (El Gaby, 2005).

REFERENCES

Abu El Ela, F.F. & Farahat, E.S., 2010. *Neoproterozoic podiform chromitites in serpentinites of the Abu Meriewa–Hagar Dungash district, Eastern Desert, Egypt: Geotectonic implications and metamorphism*. Island Arc 19, 151–164.

Abzalov, M.Z., 1998. *Chrome-spinels in gabbro-wehrlite intrusions of the Pechenga area, Kola Peninsula, Russia: emphasis on the alteration features*. Lithos 43, 109–134.

Akaad, M.K. & Abu El Ela, A.M., 1996. "*Geology and Petrochemistry of the Mueilih Submarine Metabasalts, Qift–Quseir Region, Eastern Desert"*. Egyptian Journal of Geology 40(1), 321–349.

Akaad, M.K. & Abu El Ela, A.M., 2002. "*Geology of the Basement Rocks in the Eastern Half of the Belt Between Latitudes 25○ 30′ and 26○ 30′ N, Central Eastern Desert", Egypt*. Geol. Surv. Egypt, Special Publication, 78, pp. 118.

Aly, S.M., Ghoneim, M.F. & Beniamin, N., 1995. *Geology and origin of the Gerf serpentinites, Egypt*. Egyptian Mineralogist 7, 95–108.

Arai, S. & Yurimoto, H., 1994. *Podiform chromitites of the Tari-misaka ultramafic complex, southwest Japan, as mantle–melt interaction products*. Economic Geology 89, 1279–1288.

Augé, T., 1987. *Chromite deposits in the northern Oman ophiolite: mineralogical constraints*: Mineralium Deposita 22, 1-10.

Bach, W., Gretchen, L. & Früh-Green, L. 2010. *Alteration of the oceanic lithosphere and implications for seafloor processes*. Elements 6(3), 173-178.

Bach, W., Paulick, H., Garrido, C.J., Ildefonse, B., Meurer, W. & Humphris, S.E., 2006. *Unravelling the sequence of serpentinization reactions: petrography, mineral chemistry, and petrophysics of serpentinites from MAR 15ºN* (ODP Leg 209, Site 1274). Geophysical Research Letters 25, 1467-1470.

Barnes, S.J., 2000. *Chromite in Komatiites, II. Modifications during greenschist to mid-amphibolite facies metamorphism*. Journal of Petrology 41, 387–409.

Barnes, S.J. & Roeder, P.L., 2001. *The range of spinel compositions in terrestrial mafic and ultramafic rocks*. Journal of Petrology 42, 2279–2302.

Bonatti, J. & Michael, P.J., 1989. *Mantle peridotite from continental rifts to oceanic basins to subduction zones*. Earth and Planetary Science Letters 91, 287–311.

Caruso, L.J. & Chernosky, J.V., 1979. *The stability of lizardite*. The Canadian Mineralogist, 17, 757-769.

Deer, W.A., Howei, R.A. & Zussman, J., 1992. *The Rock Forming Minerals*, second ed. Longmans, London 696pp.

Dungan, M.A., 1979. *A microprobe study of antigorite and some serpentine pseudomorphs*. The Canadian Mineralogist 17, 711–784.

El Gaby, S., 2005. *Integrated evolution and rock classification of the Pan-African belt in Egyp*t. In: Proceeding of the First Symposium. On Classification of Basement Complex of Egypt, pp. 1–9.

Evans, B.W. & Frost, B.R., 1975. *Chrome-spinel in progressive metamorphism - a preliminary analysis*. Geochimica et Cosmochimica Acta 39, 959-972.

Farahat, E.S., 2001. *Comparative petrological studies of some pillowed lavas in the Eastern Desert, Egypt*. Ph. D. Thesis, Minia University, Minia, Egypt, 251pp.

Farahat, E.S., El Mahallawi, M.M., Hoinkes, G. & Abdel Aal, A.Y., 2004. *Continental back-arc basin origin of some ophiolities from the Eastern Desert of Egypt*. Mineralogy Petrology 82, 81–104.

Früh-Green, G.L., Scambelluri, M. & Vallis, F., 2001. *O-H isotope ratios of high pressure ultramafic rocks: implications for fluid sources and mobility in the subducted hydrous mantle*. Contributions to Mineralogy and Petrology 141, 145-159.

Gorton, P.M. & Schandl, E.S., 2000. *From continents to island arcs: a geochemical index of tectonic setting for arc-related and within-plate felsic to intermediate volcanic rocks:* The Canadian Mineralogist, 38, 1065-1073.

Groppo, C., Rinaudo, C., Cairo, S., Gastalsi, D. & Compagnoni, R., 2006. *Micro-Raman spectroscopy for a quick and reliable identification of serpentine minerals from ultramafics*. European Journal of Mineralogy 18, 319-329.

Gruau, G., Bernard Griffiths, J. & Lecuyer, C., 1998. *The origin of U-shaped Rate earth patterns in ophiolite peridotites: assessing the role of secondary alteration and melt/rock reaction-Western United States*. Geochemica et Cosmochimica Acta 62, 3545-3560.

Hellebrand, E., Snow, J.E., Dick, H.J.B. & Hofmann, A.W., 2001. *Coupled major and trace elements as indicators of the extent of melting in mid-ocean-ridge peridotites*. Nature 410, 677-681.

Hey, M.H., 1954. *A new review of the chlorites*. Mineralogical Magazine 30, 277-292.

Hillier, S. & Velde, B., 1991. *Octahedral occupancy and the chemical composition of diagenetic (low-temperature) chlorites*. Clay Minerals 26,149-168

Jan, M.Q. & Windley, B.F., 1990. *Chromian spinel-silicate chemistry in ultramfic rocks of the Jijal Complex, northwest Pakistan*. Journal of Petrology 31, 67–71.

Kamenetsky, V.S., Crawford, A.J. & Meffre, S., 2001. *Factors controlling chemistry of magmatic spinel: an empirical study of associated olivine, Cr-spinel and melt inclusions from primitive rocks*. Journal of Petrology 42, 655-671.

Kimball, K.L., 1990. *Effects of hydrothermal alteration on the composition of chromian spinels*. Contributions to Mineralogy and Petrology 105, 337-346.

Li, X.P., Rahn, M. & Bucher, K., 2004. *Serpentinites of the Zermatt-Saas ophiolite complex and their texture evolution*. Journal of Metamorphic Geology 22, 159-177.

Maurel, C. & Maurel, O., 1982. *Étude experimentale de la distribution de l'aluminiun entre bain silicaté basique et spinelle chromifére. Implications pétrogénétiques: teneur en chrome des spineless*. Bulletin de Minéralogie 105, 197-202.

Mellini, M., Rumori, C. & Viti, C., 2005. *Hydrothermally reset magmatic spines in retrograde serpentinites: formation of "ferritchromit" rims and chlorite aureoles*. Contributions to Mineralogy and Petrology 149, 266-275.

Merlini, A., Grieco, G. & Diella, V., 2009. *Ferritchromite and chromian-chlorite formation in mélange-hosted Kalkan chromitite (Southern Urals, Russia)*. American Mineralogist 94, 1459–1467.

Moody, J.B., 1976. *Serpentinization: a review*. Lithos 9, 125–138.

Niu, Y., 2004. *Bulk-rock major and trace element compositions of abyssal peridotites: implications for mantle melting, melt extraction and post-melting processes beneath mid-ocean ridges*. Journal of Petrology 45, 2423-2458.

Rinaudo, C., Gastaldi, D. & Belluso, E., 2003. *Characterization of chrysotile, antigorite and lizardite by FT-Raman spectroscopy*. The Canadian Mineralogist 41, 883-890.

Sack, R.O. & Ghiorso, M.S., 1991. *Chromian spinels as petrogenetic indicators: thermodynamic and petrological applications.* American Mineralogist 76, 827–847.

Shackleton, R.M., Ries, A.C., Graham, R.H. & Fitches, W.H.,1980. *Late Precambrian ophiolitic me´lange in the Eastern Desert of Egypt*. Nature 285, 472–474.

Shen, P., Hwang, S.L., Chu, H.T. & Jeng, R.C. 1988. *STEM study of ''ferritchromit'' from the Heng-Chun chromitite*. American Mineralogist 73, 383–388.

Stern, R.J. & Gwinn, C.J. 1990. *Origin of late Precambrian intrusive carbonates, Eastern Desert of Egypt and Sudan: C, O and Sr isotopic evidence.* Precambrian Research 46, 259–272.

Stern, R.J., Johanson, P.R., Kroner, A. & Yibas, B., 2004. *Neoproterozoic ophiolites of the Arabian–Nubian Shield*. In: Kusky, T.M. (Ed.) Precambrian ophiolites and related rocks. Developments in Precambrian Geology, Elsevier, Amsterdam, 13, 95-128.

Sun, S.S. & McDonough, W.F., 1989. *Chemical and isotopic systematic of oceanic basalts: implications for mantle composition and processes*, In Saunders, A.D., Norry, M.J. (Eds.), Magmatism In the ocean basins: London, U.K., Geological Society Special Publication 42, 313-345.

Wiewióra, A. & Weiss, Z., 1990. *Crystallochemical classifications of phyllosilicates based on the unified system of projection of chemical compositions*. Clay Minerals 25, 83–92.

Wilson, M., 1989. *Igneous petrogenesis*: London, U.K., Unwin Hyman, 466pp.

Winter, J.W., 2001. *An Introduction to Igneous and Metamorphic Petrology.* Prentic-Hall Inc., Englewood Cliffs, NJ 697pp.

Wylie, A.G., Candela, P.A. & Burke, T.M., 1987. *Compositional zoning in unusual Zn-rich chromite and its bearing on the origin of the ferritchromit*. American Mineralogist 72, 413–422.

Xie, X., Byerly, G.R. & Ferrell, R.E.Jr., 1997. *Trioctahedral chlorite: crystal structure and rock composition constraints with implications to geothermometry*. Contributions to Mineralogy and Petrology 126, 275-291.

Received at: 28. 06. 2013
Revised at: 28. 09. 2013
Accepted for publication at: 03. 10. 2013
Published online at: 09. 10. 2013